IOPscience iopscience.iop.org

Home Search Collections Journals About Contact us My IOPscience

Mapping of Si/SiC p–n heterojunctions using scanning internal photoemission microscopy

This content has been downloaded from IOPscience. Please scroll down to see the full text.

2016 Jpn. J. Appl. Phys. 55 04ER15

(http://iopscience.iop.org/1347-4065/55/4S/04ER15)

View the table of contents for this issue, or go to the journal homepage for more

Download details:

IP Address: 160.193.153.220
This content was downloaded on 16/03/2016 at 04:42

Please note that terms and conditions apply.

Japanese Journal of Applied Physics **55**, 04ER15 (2016)
http://doi.org/10.7567/JJAP.55.04ER15

REGULAR PAPER

Mapping of Si/SiC p–n heterojunctions using scanning internal photoemission microscopy

Masato Shingo[1], Jianbo Liang[2], Naoteru Shigekawa[2], Manabu Arai[3], and Kenji Shiojima[1*]

[1]*Graduate School of Electrical and Electronics Engineering, University of Fukui, Fukui 910-8507, Japan*
[2]*Graduate School of Engineering, Osaka City University, Osaka 558-8585, Japan*
[3]*New Japan Radio Co., Ltd., Fujimino, Saitama 356-8510, Japan*

*E-mail: shiojima@u-fukui.ac.jp

Received October 5, 2015; revised December 4, 2015; accepted December 8, 2015; published online March 9, 2016

We demonstrated the two-dimensional characterization of p^+-Si/n^--SiC heterointerfaces by scanning internal photoemission microscopy (SIPM). In internal photoemission spectra, a linear relationship was found between the square root of photoyield (Y) and photon energy, and the threshold energy (qV_{th}) was reasonably obtained to be 1.34 eV. From the SIPM results, Y and qV_{th} maps were successfully obtained, and nanometer-deep gaps in the junction were sensitively visualized as a pattern. These results suggest that this method is a powerful tool for investigating the inhomogeneity of heterojunctions as well as their carrier transport properties. © 2016 The Japan Society of Applied Physics

1. Introduction

GaN- and SiC-based devices are promising next-generation power devices because of their unique physical properties such as a wide band gap, a high thermal conductivity, a high electron saturation velocity, high physical and chemical stabilities, and a high breakdown field. GaN has the advantages of the formation of heterojunctions with AlGaN and InGaN, and their spontaneous and piezopolarizations, which induce two-dimensional electron gases at the heterointerfaces. Thus, AlGaN/GaN high-electron-mobility transistors (HEMTs) have been intensively studied and practically developed for power amplifiers of base stations.[1] Recently, free-standing bulk GaN substrates have been commercially available. Consequently, several novel devices such as vertical field-effect transistors (FETs), p–n junctions, and Schottky diodes have been demonstrated.[2]

On the other hand, bulk crystals of SiC are grown by the sublimation method and SiC-based metal–insulator-semiconductor (MOS) structures are formed by the thermal oxidation process. Therefore, Schottky diodes and MOSFETs have been established. The combination of SiC with Si technologies has potential application for heterojunction bipolar transistors as next-generation power devices.[3,4] In growing SiC layers on Si,[5] however, a marked amount of residual stress and a considerable number of defects with high densities are frequently encountered owing to the large lattice mismatch and difference in thermal expansion coefficient between Si and SiC, which limits the intrinsic performance of grown Si/SiC heterojunctions.[6]

A wafer bonding technique would be a breakthrough on this problem. In general, wafer bonding techniques have been widely used for the fabrication of three-dimensional large-scale integrated circuits[7] and optical electrical integrated circuits,[8] and for a better thermal dispersion from a mounted circuit to a bonded substrate, thus far.[9] As a next generation of development, recently, bonding interfaces have been used as active parts in the devices, typically seen in hybrid tandem solar cells.[10]

It is notable that the reported conduction band discontinuities in Si/SiC heterojunctions fabricated by a conventional bonding method are largely scattered between 0.21 and 1.9 eV.[5,11] This suggests that the electrical properties of the Si/SiC heterojunctions largely vary with surface wet chemical treatment and possible interface states.

Such uncertainties stemming from the wet process are assumed to be rendered in direct wafer bonding processes[12–14] such as surface-activated bonding (SAB)[15,16] since substrates are bonded without using the wet process. Surfaces of substrates are activated by the fast atom beams of Ar prior to SAB, which enables us to bond substrates without heating them.[17–25] We have fabricated p-Si/n-SiC and n-Si/n-SiC heterojunctions by SAB and found that the flat band voltage is ~0.92 eV from current–voltage (I–V) measurements.[26] However, interface states with high densities are likely to be formed in the SAB process since dangling bonds are unveiled on sample surfaces owing to the irradiation of Ar atom beams. The impact of the interface states to the electrical properties of Si/SiC junctions has not yet been fully understood.

To develop practical devices including an active bonding interface, a near-ideal interface is required, but as mentioned above, actual interfaces suffer from some material and technical problems: (i) surface roughness, interfacial states, and damage, (ii) surface treatment for eliminating the remaining contaminated oxide layers, and (iii) uniform pressure on bonding with a high-precision machine and complete parallel wafers. Because these factors would induce inhomogeneity in the interface, two-dimensional characterization is required for the practical device development.

We have developed a novel two-dimensional mapping characterization method, scanning internal photoemission microscopy (SIPM), to verify the electrical inhomogeneity of metal/semiconductor (M/S) interfaces. To date, we have successfully demonstrated the mapping of thermal degradation and surface damage in Si, GaAs, SiC, and GaN Schottky contacts.[27–29]

In this study, we have applied this technique to characterize p^+-Si/n^--SiC heterointerfaces. After verifying the validity of using the internal photoemission effect for a heterointerface was shown, SIPM mapping was conducted to reveal the interfacial roughness.

2. Experimental methods

We prepared 525-μm-thick B-doped p^+-Si (100) ($N_A = 2.6 \times 10^{19}\,cm^{-3}$) substrates and 10-μm-thick n^--SiC ($N_D = 5.4 \times$

© 2016 The Japan Society of Applied Physics

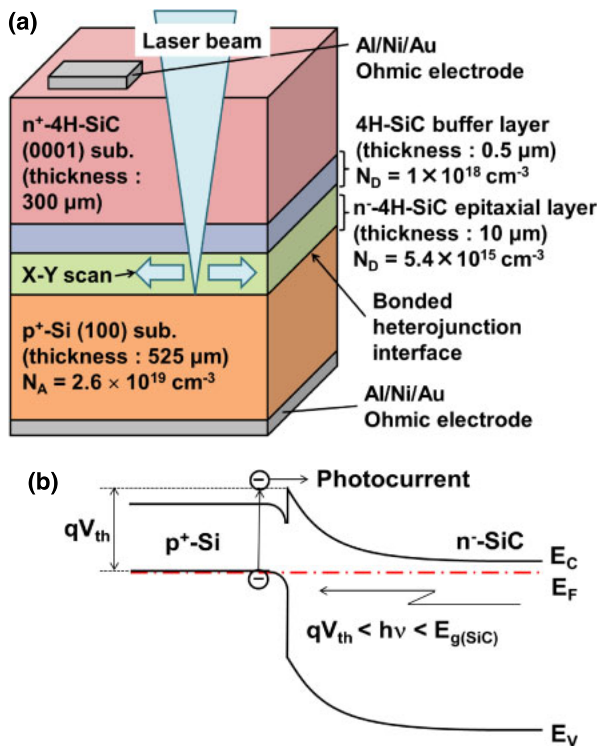

Fig. 1. (Color online) (a) Device structure and (b) energy band diagram of p^+-Si/n^--SiC heterojunction.

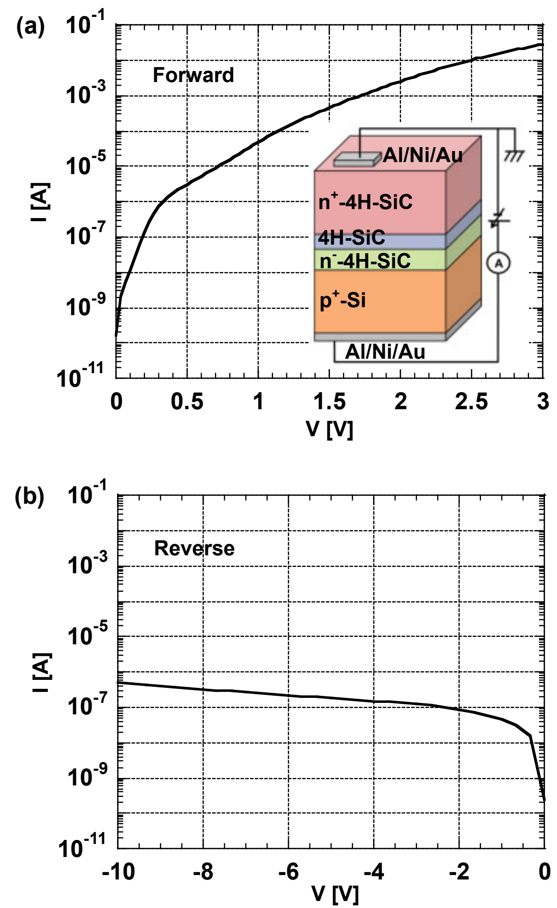

Fig. 2. (Color online) (a) Forward and (b) reverse *I*–*V* characteristics of the p^+-Si/n^--SiC heterojunction.

$10^{15}\,\mathrm{cm^{-3}}$) epitaxial layers/0.5-µm-thick 4H-SiC ($N_D = 1.0 \times 10^{18}\,\mathrm{cm^{-3}}$) buffer layers grown on a 300-µm-thick n^+-4H-SiC (0001) substrate, as shown in Fig. 1(a). The 4H-SiC substrate has an off-angle of 4° toward the [11$\bar{2}$0] direction. Al/Ni/Au multilayers for ohmic contacts were evaporated on the back surfaces of p^+-Si and n^+-SiC substrates. We polished the surfaces of the SiC substrates so as to remove the undulation that we had originally observed on the surfaces. Then, we bonded the p-type substrate to the SiC epitaxial substrate by SAB to fabricate p^+-Si/n^--SiC junctions. The SAB process used was previously reported in detail in Refs. 25 and 30. Finally, the ohmic contacts on p-type Si and n-type SiC were sintered by rapid thermal annealing at 800 °C for 60 s in N_2 gas ambient. We measured the *I*–*V* characteristics by using a semiconductor parameter analyzer (HP4142B) to confirm basic diode behavior.

Prior to the SIPM measurements, we conducted conventional photoresponse (PR) measurements, where a photocurrent was detected while photon energy ($h\nu$) was continuously scanned. The original PR measurement is based on the internal photoemission effect, which is valid for a M/S interface. The relationship between $h\nu$ and photoyield (Y), corresponding to the photocurrent per number of incident photons, is given by Fowler's equation:[31]

$$Y^{1/2} \propto h\nu - q\phi_B, \tag{1}$$

where $q\phi_B$ is the Schottky barrier height. In this study, we applied the internal photoemission measurements to a semiconductor/semiconductor (S/S) heterointerface. As shown in Fig. 1(b), a p^+/n^- junction was prepared to form a similar band diagram to a M/S interface. We define threshold energy (qV_{th}) as the energy difference from the top of the valence band of the p-Si side to the bottom of the conduction band of the n-SiC side at the interface. When a monochromatic light with an energy $h\nu$ above qV_{th} but below the energy band gap of SiC is incident on the interface, electrons around the Fermi level (E_F) in p-Si are excited, and can surmount the barrier generating a photocurrent under the electrical field in the depletion layer. When $h\nu$ is close to the fundamental absorption edge of SiC, a large photocurrent flows owing to electron–hole pair generation as in a solar cell. In the SIPM measurements, one focuses and scans the beam over the interface in a $200 \times 200\,\mathrm{\mu m^2}$ area for obtaining a two-dimensional image of Y. Red ($\lambda_1 = 660$ nm, $h\nu_1 = 1.88$ eV) and green ($\lambda_2 = 516$ nm, $h\nu_2 = 2.40$ eV) light lasers were used in this study. Finally, we observed the SiC surface before bonding by atomic force microscopy (AFM).

3. Results and discussion

The *I*–*V* characteristics of the p^+-Si/n^--SiC heterojunction are shown in Fig. 2, where the ohmic contact on the SiC side is grounded. The respective curves revealed a rectifying property. The current values at +3 and −10 V are different by about 5 orders of magnitude.

Figure 3 shows typical PR spectra plotted in a square root of Y in the same manner as the M/S interface. As expected, a photocurrent was detected even in the p^+-Si/n^--SiC heterojunction. A large peak at the fundamental absorption edge near the band gap of SiC was observed. In addition, on the lower $h\nu$ side of the peak, a linear portion can be seen between 1.4 and 2.5 eV. In this device structure, the incident

© 2016 The Japan Society of Applied Physics

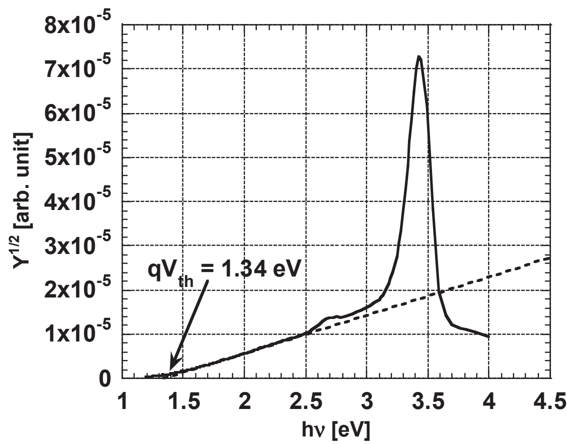

Fig. 3. PR spectra of the p^+-Si/n^--SiC heterojunction.

photons are absorbed in the vicinity of the Si surface at the interface, and electrons in the valence band are excited across the energy band gap of Si. Because of the indirect band structure of Si, the absorption coefficient has a wavelength dispersion of square root. Therefore, this would be responsible for the linear relationship. Since the electrons excited around E_F contribute to the photocurrent, the onset energy of the spectra would be qV_{th}. From these experimental results, we can empirically rewrite Eq. (1) to

$$Y^{1/2} \propto h\nu - qV_{th}. \tag{2}$$

The qV_{th} was obtained to be 1.34 eV. This value is in good agreement with our previously reported value obtained from the C–V results.[26] We confirmed that PR measurement is effective for determining qV_{th}. We also confirmed that, because the two laser wavelengths in the SIPM measurements are within the linear portion in the PR spectra, the choice of wavelengths is reasonable for determining qV_{th}.

We show the SIPM results in Figs. 4(a) and 4(b). The Y map at $\lambda_2 = 516$ nm [Fig. 4(a)] revealed randomly oriented sharp lines and aligned trenches, which corresponded to small Y signals. We repeated the same measurement at $\lambda_1 = 660$ nm, and the qV_{th} image was obtained according to Eq. (2). Basically, the same pattern was also observed in the qV_{th} map in Fig. 4(b), and qV_{th} was obtained to be 1.34 eV in regions without lines and trenches. As expected, the qV_{th} from the SIPM result is consistent with that from the PR results.

To reveal the origin of the pattern, AFM measurements were conducted at the SiC surface before bonding. A similar pattern can be observed in the AFM image as shown in Fig. 5. Typical randomly oriented sharp lines are 1–5 nm deep and about 1 µm wide. The sharp lines are considered to be scratches formed upon polishing the SiC wafer. Even in nanometer-deep scratches, a gap can be formed between Si and SiC in the junction; thus, the photocurrent was not detected in these regions. In the AFM image, the aligned trench pattern was not clearly observed, but the pattern is probably caused by the step bunching of the SiC surface, because the trenches are aligned toward the same direction as the off-angle of the SiC substrate. These results tell us that SIPM is suitable for not only M/S contacts but also S/S heterojunctions, and significantly sensitive to a nanometer-order surface morphology.

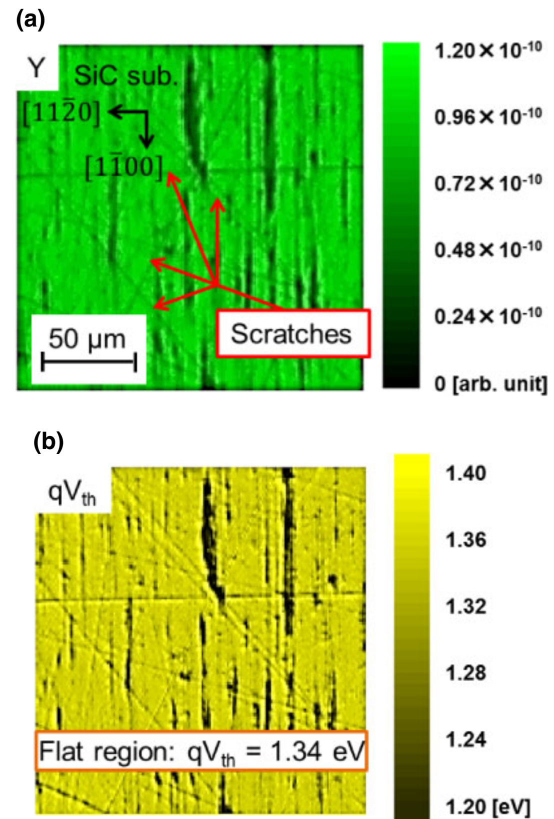

Fig. 4. (Color online) (a) Y ($\lambda = 516$ nm) and (b) qV_{th} maps of the p^+-Si/n^--SiC heterojunction by SIPM.

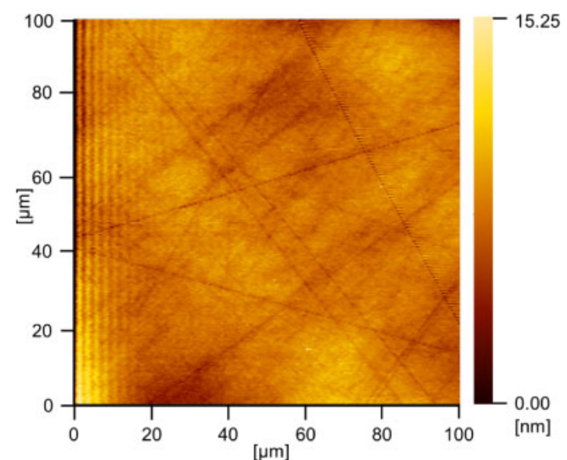

Fig. 5. (Color online) AFM image of the SiC epitaxial layer surface before bonding.

4. Conclusions

The p^+-Si/n^--SiC heterojunctions were characterized by I–V, PR, and SIPM measurements. In PR spectra, a linear relationship was found between $Y^{1/2}$ and $h\nu$, and qV_{th} was reasonably obtained to be 1.34 eV. In SIPM results, Y and qV_{th} maps were successfully obtained, and nanometer-deep scratches in the junction were sensitively visualized as a pattern. We confirmed that this method is a powerful tool for investigating the inhomogeneity of the heterojunctions as well as their carrier transport properties.

© 2016 The Japan Society of Applied Physics

Acknowledgments

Part of this work was supported by a Grant-in-Aid for Scientific Research C (15K05981) of the Ministry of Education, Culture, Sports, Science and Technology. The authors would like to thank Professor Kenji Hisada of University of Fukui for the AFM observation.

1) T. Kikkawa, Jpn. J. Appl. Phys. **44**, 4896 (2005).
2) K. Nomoto, Y. Hatakeyama, H. Katayose, N. Kaneda, T. Mishima, and T. Nakamura, Phys. Status Solidi A **208**, 1535 (2011).
3) T. Sugii, T. Ito, Y. Furumura, M. Doki, F. Mieno, and M. Maeda, IEEE Electron Device Lett. **9**, 87 (1988).
4) T. Sugii, T. Yamazaki, and T. Ito, IEEE Trans. Electron Devices **37**, 2331 (1990).
5) A. Pérez-Tomás, M. R. Jennings, M. Davis, J. A. Covington, P. A. Mawby, V. Shah, and T. Grasby, J. Appl. Phys. **102**, 014505 (2007).
6) A. N. Nazarov, Ya. N. Vovk, V. S. Lysenko, V. I. Turchanikov, V. A. Scryshevskii, and S. Ashok, J. Appl. Phys. **89**, 4422 (2001).
7) A. Jourdain, S. Stoukatch, P. De Moor, and W. Ruythooren, Proc. IITC, 2007, p. 207.
8) Y. Okuno, M. Aoki, T. Tsuchiya, and K. Uomi, Appl. Phys. Lett. **67**, 810 (1995).
9) W. K. Chan, Jpn. J. Appl. Phys. **37**, 813 (1998).
10) N. Shigekawa, J. Liang, R. Onitsuka, T. Agui, H. Juso, and T. Takamoto, Jpn. J. Appl. Phys. **54**, 08KE03 (2015).
11) H. Hanafusa, A. Ohta, R. Ashihara, K. Maruyama, T. Mizuno, S. Hayashi, H. Murakami, and S. Higashi, Mater. Sci. Forum **778–780**, 649 (2014).
12) M. R. Jennings, A. Pérez-Tomás, O. J. Guy, R. Hammond, S. E. Burrows, P. M. Gammon, M. Lodzinski, J. A. Covington, and P. A. Mawby, Electrochem. Solid-State Lett. **11**, H306 (2008).
13) A. Pérez-Tomás, M. Lodzinski, O. J. Guy, M. R. Jennings, M. Placidi, J. Llobet, P. M. Gammon, M. C. Davis, J. A. Covington, S. E. Burrows, and P. A. Mawby, Appl. Phys. Lett. **94**, 103510 (2009).
14) M. Yoshimoto, R. Araki, T. Kurumi, and H. Kinoshita, ECS Trans. **50** [7], 61 (2013).
15) J. Liang, S. Nishida, M. Arai, and N. Shigekawa, Appl. Phys. Lett. **104**, 161604 (2014).
16) S. Nishida, J. Liang, T. Hayashi, M. Arai, and N. Shigekawa, Jpn. J. Appl. Phys. **54**, 030210 (2015).
17) H. Takagi, K. Kikuchi, R. Maeda, T. R. Chung, and T. Suga, Appl. Phys. Lett. **68**, 2222 (1996).
18) H. Takagi, R. Maeda, T. R. Chung, N. Hosoda, and T. Suga, Jpn. J. Appl. Phys. **37**, 4197 (1998).
19) H. Takagi, R. Maeda, N. Hosoda, and T. Suga, Jpn. J. Appl. Phys. **38**, 1589 (1999).
20) M. M. R. Howlader, T. Watanabe, and T. Suga, J. Appl. Phys. **91**, 3062 (2002).
21) C. Wang, E. Higurashi, and T. Suga, Jpn. J. Appl. Phys. **47**, 2526 (2008).
22) M. M. R. Howlader, T. Watanabe, and T. Suga, J. Vac. Sci. Technol. B **19**, 2114 (2001).
23) N. Shigekawa, N. Watanabe, and E. Higurashi, Proc. 3rd Int. IEEE Workshop Low-temperature Bonding for 3D Integration, 2012, p. 109.
24) J. Liang, T. Miyazaki, M. Morimoto, S. Nishida, N. Watanabe, and N. Shigekawa, Appl. Phys. Express **6**, 021801 (2013).
25) J. Liang, T. Miyazaki, M. Morimoto, S. Nishida, and N. Shigekawa, J. Appl. Phys. **114**, 183703 (2013).
26) J. Liang, S. Nishida, T. Hayashi, M. Arai, and N. Shigekawa, Appl. Phys. Lett. **105**, 151607 (2014).
27) T. Okumura and K. Shiojima, Jpn. J. Appl. Phys. **28**, L1108 (1989).
28) K. Shiojima and T. Okumura, J. Cryst. Growth **103**, 234 (1990).
29) K. Shiojima, S. Yamamoto, Y. Kihara, and T. Mishima, Appl. Phys. Express **8**, 046502 (2015).
30) N. Shigekawa, J. Liang, and N. Watanabe, Proc. 39th IEEE Photovoltaic Specialists Conf., 2013, p. 2470.
31) R. H. Fowler, Phys. Rev. **38**, 45 (1931).

© 2016 The Japan Society of Applied Physics